Effect of Uniaxial Stress on Excitons Bound to Bismuth in GaP†

A. ONTON AND T. N. MORGAN
IBM Watson Research Center, Yorktown Heights, New York 10598
(Received 19 September 1969)

We have studied the effects of uniaxial compression on the zero-phonon photoluminescence spectrum of excitons bound to bismuth impurities in GaP at liquid-helium temperatures. The quantitative stress dependence is consistent with the exciton being associated primarily with the ⟨100⟩ conduction-band minima. The valley-orbit interaction is shown to lower the energy of the singlet, symmetric valley combination of the exciton, and the valley-orbit splitting is estimated to be 30 meV. The polarization of the emission with uniaxial stress applied to the sample, and the stress dependence of the emission lines, are only qualitatively consistent with the j-j coupling model of the exciton. The deformation potentials D_u and D_u' for the $J=1$ state of the exciton are measured to be 0.17 and 0.8 eV, respectively, approximately an order of magnitude smaller than the corresponding free-hole deformation potentials and about one-half those of the $J=2$ state. The $J=2$ state is observed to be split by $\sim$0.25 meV into a higher Γ_3 and a lower Γ_4 level. This splitting, as well as other inconsistencies with the simple model, is attributed in part to the dynamic Jahn-Teller effect.

I. INTRODUCTION

LUMINESCENCE from bismuth-doped gallium phosphide has been studied by Trumbore, Gershenzon, and Thomas,[1] and by Hopfield, Thomas, and Lynch[2] and identified in the latter work with the decay of excitons bound to isolated Bi impurities which occur substitutionally on P sites. The exciton was observed to be a doublet with the 2.7-meV separation of the two components ascribed to j-j (exchange) coupling between the $p_{3/2}$ hole and $s_{1/2}$ electron states. This is similar to the weakly bound exciton associated with nitrogen impurities identified earlier by the same workers.[3,4] Zero-phonon emission from the lower-lying $J=2$ state was found to be dipole forbidden and that from the higher $J=1$ state allowed. Strong phonon replicas of both transitions were seen.

According to the model proposed by Thomas *et al.*,[3] the observed exciton is composed primarily of hole states from near the valence band maximum and of electron states from near the minima of the ⟨100⟩ conduction band valleys. The electron states were assumed to undergo a "normal" valley-orbit splitting as a result of interactions with the impurity core, although the sign and magnitude of this splitting were not determined experimentally. In addition, the strength and richness of the vibronic structure reported in Refs. 1 and 2 indicate that the exciton is strongly coupled to the lattice, although the small binding energy of $\sim$100 meV suggests a state in which the electron and hole wave functions are diffuse and in which the coupling to the lattice is small. This contradiction and the incompleteness of our knowledge of the exciton states make it apparent that further study of the Bi exciton in GaP is needed.

Consequently, as described in Sec. II, we have measured the stress dependence of photoluminescence from Bi excitons in GaP. We develop in Sec. III the theory of bound exciton states in a stressed crystal. Our experimental results are presented in Sec. IV and interpreted in Sec. V with the following major conclusions:

(1) The electron part of the observed exciton states is found to be a "normal" valley-orbit split singlet formed from the ⟨100⟩ conduction band valleys, with the singlet lying approximately 30 meV below the doublet.

(2) The stress dependence and polarization of the emitted radiation are found to be in qualitative agreement with the original model of an exciton bound to a point defect, although some quantitative discrepancies exist.

(3) The exciton is found to exhibit a small crystal field splitting of its $J=2$ level and to be split under stress by an amount much smaller than that predicted from known band-edge deformation potentials.

(4) The splitting is found to be anisotropic relative to stresses in the ⟨111⟩ and ⟨100⟩ directions with a ratio of about 2.5:1 and to be larger for the B line ($J=2$) than for the A line ($J=1$) by a factor of 2.

II. EXPERIMENTAL PROCEDURE

The samples used were cut from platelets of solution grown GaP containing the impurity Bi. One sample [GaP(Bi) ML641-ZB38] was prepared by making a bismuth-doped epitaxial solution overgrowth on a large single crystal of GaP. The crystallographic orientation of the finished samples was checked using x rays. The samples were etched in aqua regia prior to measurement.

The measurements were made by observing the photoluminescence excited by light of 4880 or 5145 Å wavelength from an argon ion laser with a nominal power output of about 1-W cw. The emitted light was analyzed by either a Perkin-Elmer model 99-G double-

† A preliminary account of these results was presented by A. Onton and T. N. Morgan, Bull. Am. Phys. Soc. **14**, 26 (1969).

[1] F. A. Trumbore, M. Gershenzon, and D. G. Thomas, Appl. Phys. Letters **9**, 4 (1966).

[2] J. J. Hopfield, D. G. Thomas, and R. T. Lynch, Phys. Rev. Letters **17**, 312 (1966).

[3] D. G. Thomas, M. Gershenzon, and J. J. Hopfield, Phys. Rev. **131**, 2397 (1963).

[4] D. G. Thomas, J. J. Hopfield, and C. J. Frosch, Phys. Rev. Letters **15**, 857 (1965).

pass monochromator together with a photomultiplier tube with an S-20 characteristic or a Bausch and Lomb 2-m spectrograph. These instruments were equipped with gratings blazed for 5000 Å and having 1800 or 1200 lines/mm, respectively. With the Perkin-Elmer system, relative intensities of light emitted with electric vector parallel and perpendicular to the stress axis were measured by using a polaroid sheet followed by a half-wave plate at the entrance slit of the monochromator. The sample was mounted in a Dewar on a device by which uniaxial compression could be both applied and measured from outside the Dewar. The optical windows in the tail of the Dewar were of fused quartz. The sample could be immersed in liquid helium, or maintained at a higher temperature by a controlled flow of cold helium gas.

III. EXCITON STATES

A. Basis States

The theory of bound exciton states in semiconductors has been developed by Thomas and co-workers.[1–4] In the case of the Bi exciton in GaP the hole is bound to the neutral Bi core by short-range forces, and the electron is bound to the hole by Coulomb forces.[5] The exchange part of the Coulomb binding energy, the j-j coupling, produces a splitting between the exciton states having parallel and antiparallel electron and hole spins.

The hole states are formed from the top of the valence band near the center of the Brillouin zone and transform according to the Γ_8 irreducible representation of the T_d double point group.[6] They resemble $p_{3/2}$ atomic states, and the core part of each wave function can be written as a radial part times products of the $l=1$ spherical harmonics $Y_1{}^m(\theta,\phi)$ and the two-hole spin functions. The coefficients of these products are the Wigner or Clebsch-Gordan coefficients.[7] The electron states resemble hydrogenic donor states formed from the three conduction-band minima at X. The band states (without spin) transform as X_1 about the impurity site but are mixed and split by the attractive potential of the bound hole into a symmetric Γ_1 singlet and a Γ_3 doublet.[8] With spin the singlet transforms as Γ_6 and resembles an $s_{1/2}$ atomic state.

We find experimentally (see Sec. V) that the ground state is the singlet (Γ_1) and not the doublet (Γ_3) and hence that the exciton exhibits a "normal" valley-orbit splitting.[8] This occurs even though the Bi-impurity potential is expected to be repulsive for electrons[2] and hence should raise the energy of the symmetric Γ_1 state. It is due to the fact that the electron is bound by its interaction with the hole which is not highly localized near the Bi. Hence the "core" potential which generates the valley-orbit splitting arises from the reduced dielectric constant (dielectric breakdown) very near the hole and not from the impurity core itself. This conclusion emphasizes the fact that unusual circumstances are required to produce an "inverted" valley-orbit splitting of states bound by Coulomb forces.

Because of their similarity to $s_{1/2}{}^+$ and $p_{3/2}{}^-$ atomic functions (where + and − indicate their parity),[9] the electron and hole couple to form two states, a $J=1$ triplet of energy $E=E_0+(5/8)\Delta$ and at a lower energy a $J=2$ quintet of energy $E=E_0-(3/8)\Delta$ (see Fig. 1). The center-of-gravity energy E_0 equals the band gap E_g minus the exciton binding energy. The basis functions for these states may be taken to be $|J,M\rangle$ atomic states of (−) parity with $J=1$ and 2. The energy difference $\Delta\approx 2.7$ meV between the states depends upon both the electron-hole overlap and the exchange interaction between the core functions.[10] For an exchange interaction of $I_0=1$ eV estimated from atomic spectroscopic data, the observed splitting is consistent with a hydrogenic overlap function having a Bohr radius of

$$a_0=12\text{ Å},$$

a reasonable value. The selection rules for radiative decay from these states are well known—only the $J=1$ states emit radiation, and the polarization of the light is parallel to the quantization axis for $M=0$ but perpen-

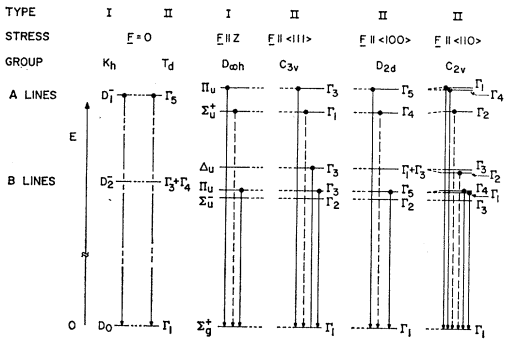

FIG. 1. A schematic diagram showing the energy levels and their group representations for an exciton in a tetrahedral crystal. Type-I states are based on the effective symmetry when the T_d crystal field may be neglected, while type-II states refer to the exact symmetry of the system—see text. The groups appropriate to the indicated stresses are labeled, and the allowed transitions to the ground state are identified by arrows. Solid arrows indicate σ polarization relative to the stress axis, dashed arrows indicate π polarization, and mixed arrows indicate both polarizations. The transition in C_{3v} shown with a headless arrow is allowed only by virtue of coupling through the crystal field.

[5] P. J. Dean, J. D. Cuthbert, and R. T. Lynch, Phys. Rev. **179**, 754 (1969).

[6] G. F. Koster, J. O. Dimmock, R. G. Wheeler, and H. Statz, *Properties of the Thirty-Two Point Groups* (MIT Press, Cambridge, Mass., 1965). The notation in this book will be used throughout.

[7] V. Heine, *Group Theory in Quantum Mechanics* (The Macmillan Co., New York, 1964).

[8] See the discussion of donor states in Ge and Si by W. Kohn, in *Solid State Physics*, edited by F. Seitz and D. Turnbull (Academic Press Inc., New York, 1957), Vol. 5, p. 257, and of the symmetry of donor states in GaP by T. N. Morgan, Phys. Rev. Letters **21**, 819 (1968).

[9] E. V. Condon and G. H. Shortley, *The Theory of Atomic Spectra* (Cambridge University Press, Cambridge, England, 1951).

[10] R. J. Elliot, in *Polarons and Excitons*, edited by C. G. Kuper and G. D. Whitfield (Plenum Press, Inc., New York, 1963).

dicular to this axis for $M=\pm 1$. The changes induced by stress in the energies and transition probabilities of these states are discussed in Sec. III C following consideration of the effects of the crystal field.

B. Crystal Field

The effect of the crystal field is in general a mixing of the exciton basis states with each other and with higher-lying states and hence a splitting of the $J=2$ state into a Γ_3 doublet and a Γ_4 triplet. As discussed by Morgan and Morgan,[11] since each basis state is formed from a combination of one p-like and one s-like state, there is no mixing within the set of 12 exciton states (including four from the spin-orbit split valence band) by the spin-independent T_d crystal field, and hence the crystal-field splitting is expected to be small. The $J=2$ exciton state thus differs essentially from the orbital D states treated in crystal-field theory texts[12] and has a zero first-order crystal-field splitting, i.e.,

$$D_q=0.$$

The above conclusion that the crystal-field splitting is negligible is contradicted by the experimental results we report below which show that the $\Gamma_3-\Gamma_4$ splitting equals about 10% of the $\Gamma_5-\Gamma_4$ separation. Because of the smallness of the splitting we omit it from our calculations in order to simplify them. If desired, its effect can be introduced by perturbation theory. A brief discussion of the stress dependence of the Γ_3 and Γ_4 levels is given at the end of this section.

Although it is conceivable that a crystal-field splitting could arise from higher-order effects of the static crystal field, it is considered more probable that it has a different origin. The true states of the exciton are not pure electronic states but are vibronic states by virtue of the dynamic Jahn-Teller effect resulting from coupling between the hole and localized lattice distortions of type $\Gamma_5\equiv T_2$ and $\Gamma_3\equiv E$. Preliminary calculations of the consequences of this coupling have been made and indicate that it can generate $\Gamma_3-\Gamma_4$ splittings of the sign and magnitude observed and can explain many of the discrepancies between the theory developed here and the experimental results. The details of this calculation will be published separately by one of the authors.[13] We shall only list here the consequences which are relevant to the present work.

(1) The dyanmic Jahn-Teller effect transforms the lowest electronic states into vibronic states of the same symmetries (within the T_d group) and causes a quenching (reduction) of various coupling parameters such as the effective deformation potentials which describe splitting of the states under stress.

(2) The observed $\Gamma_3-\Gamma_4$ splitting can be explained by vibronic coupling since the exciton is found to be more strongly coupled to lattice distortions of type T_2 than to those of type E.

(3) This coupling difference generates a corresponding anisotropy in the effective deformation potentials and increases the anisotropy ratio β; see Eq. (12).

(4) The quenching of the stress coefficients is in general greater for the $J=1$ state which lies closer in energy to the excited vibrational states with which it mixes than for the lower $J=2$ state.

(5) The additional coupling to the E modes through the $\langle 100\rangle$ valleys of the conduction band modifies the apparent valley-orbit splitting, especially at small applied external stress.

C. Stress Dependence

In the absence of coupling to the crystal field, the Hamiltonian of the exciton in the undistorted crystal has the effective symmetry of the complete rotation group K_h. In the presence of an axial stress field along either a $\langle 100\rangle$ or a $\langle 111\rangle$ axis this symmetry is reduced to $D_{\infty h}$, though the true symmetry including coupling to the crystal depends upon the orientation of the stress relative to the crystal axes. The symmetries of the Hamiltonian and the classification of the states with and without applied stress are summarized in Fig. 1. They are shown both with and without coupling to the crystal field—labeled type II and type I, respectively. For the case of $\langle 110\rangle$ stress we find that the stress-induced potential is not in general axial, and that the states can best be analyzed in terms of the correct C_{2v} symmetry group.

1. *Isotropic Coupling*

The stress field produced in a homogeneous material by a uniaxial compressive force $\mathbf{F}$ can be resolved into the sum of a hydrostatic pressure

$$P=\tfrac{1}{3}F \tag{1}$$

and a uniaxial shear described by a stress tensor $\boldsymbol{\tau}$.[14,15] The former is invariant under rotations of the coordinate system and changes only the center-of-gravity energy E_0 of the exciton,[16–18]

$$\Delta E_0=-(\Xi_d+D_d^v+\Xi_u/3)(s_{11}+2s_{12})F. \tag{2}$$

Here, ΔE_0 is the change in exciton energy due to hydrostatic pressure; Ξ_d and D_d^v are the hydrostatic deformation potentials of the bound electron and hole, re-

[11] J. van W. Morgan and T. N. Morgan, Phys. Rev. (to be published).
[12] See, for example, C. J. Ballhausen, *Introduction to Ligand Field Theory* (McGraw-Hill Book Co., New York, 1962), Chap. 4.
[13] T. N. Morgan, J. Luminescence 1, 420 (1969).
[14] F. C. Von der Lage and H. A. Bethe, Phys. Rev. **71**, 612 (1947).
[15] Cf. I. S. Sokolnikoff, *Mathematical Theory of Elasticity* (McGraw-Hill Book Co., New York, 1946).
[16] W. H. Kleiner and L. M. Roth, Phys. Rev. Letters **2**, 334 (1959).
[17] C. Herring and E. Vogt, Phys. Rev. **101**, 944 (1956).
[18] G. E. Picus and G. L. Bir, Fiz. Tverd. Tela **1**, 1642 (1959) [English Transl.: Soviet Phys.—Solid State **1**, 1502 (1959)].

spectively; Ξ_u is the shear deformation potential of the multivalley conduction band; and s_{11} and s_{12} are the elastic compliance coefficients of the crystal.

The components of τ transform as the spherical harmonics $Y_2^m(\theta,\phi)$ and can split the valence band and lift the degeneracies of the exciton levels. In particular, in a coordinate system having its z axis along $\mathbf{F}$, τ is diagonal with components corresponding to those of $Y_2^0(\theta)$,

$$\tau_{ii}=(1,\,1,\,-2)F/3\,,\quad i=x,\,y,\,z. \tag{3}$$

The effects of this shear stress arise from a splitting 2ϵ between the $|m|=\frac{1}{2}$ and $|m|=\frac{3}{2}$ branches of the $p_{3/2}$ valence band and a mixing and splitting of the valley-orbit split sublevels of the multivalley electron ground state.

The theory of the electron states is described in Appendix A and the strain dependence of their energies is shown in Fig. 13. Since, as we show in Sec. V, the valley-orbit splitting E_{12} is large compared to kT and the singlet state lies lowest, the effect of shear stress on the electron part of the exciton is to produce an energy shift which depends on the orientation of the stress axis with respect to the conduction band valley axes. In effect, it introduces a center of gravity shift of the populated exciton levels which is zero for a $\langle 111\rangle$ stress and hence differs from the isotropic shift produced by hydrostatic pressure.

The splitting of the valence band under stress separates the $J=1$ and $J=2$ states into sets of sublevels—one for each value of $|M|$ (quantized along the stress)—and mixes those having $|M|=1$. This splitting 2ϵ is proportional (with coefficient B) to the axial component of stress, $T<0$, when its direction coincides with the quantization axis of M,[19]

$$\epsilon=-BT=B(\tfrac{2}{3}F) \tag{4a}$$

or to the corresponding strain component $S=s^*T$,

$$\epsilon=-DS. \tag{4b}$$

Here s^* is the appropriate elastic compliance coefficient. The effective strain potential V_s which generates these effects is derived from τ and, for isotropic coupling between the stress and the valence band, may be written

$$V_s=(20\pi)^{1/2}Y_2^0(\theta)BT. \tag{5}$$

The energies of the levels are easily determined for the exciton functions from the matrix elements of V_s. For the $|M|=1$ states, the only ones mixed by strain in isotropic material, the energies are the eigenvalues of the 2×2 matrix given by Eq. (6).

In the basis $|1,\pm1\rangle$, $|2,\pm1\rangle$, with $\epsilon=B(\frac{2}{3}F)$ the matrix is

$$\mathbf{M}_{\pm1}=\begin{pmatrix}(5\Delta/8)+\frac{1}{2}\epsilon & \pm\frac{1}{2}\sqrt{3}\epsilon\\ \pm\frac{1}{2}\sqrt{3}\epsilon & -(3\Delta/8)-\frac{1}{2}\epsilon\end{pmatrix}. \tag{6}$$

The energies $E(J,M)$ are

$$E(1,\pm1)=E_0+(\Delta/8)+(\tfrac{1}{4}\Delta^2+\tfrac{1}{2}\Delta\epsilon+\epsilon^2)^{1/2},\quad \pi \tag{7a}$$

$$E(1,0)=E_0+(5\Delta/8)-\epsilon,\quad \Sigma^+ \tag{7b}$$

$$E(2,\pm2)=E_0-(3\Delta/8)+\epsilon,\quad \Delta \tag{7c}$$

$$E(2,\pm1)=E_0+(\Delta/8)-(\tfrac{1}{4}\Delta^2+\tfrac{1}{2}\Delta\epsilon+\epsilon^2)^{1/2},\quad \pi \tag{7d}$$

$$E(2,0)=E_0-(3\Delta/8)-\epsilon,\quad \Sigma^- \tag{7e}$$

where the labels J in $E(J,\pm1)$ identify the limiting states as $\epsilon\to0$. The labels $\Sigma^\pm$, π, and Δ on the right in Eqs. (7) identify the irreducible representations of the axial group to which the wave functions belong.[14]

The energies of these states as a function of the valence band splitting parameter ϵ [see Eq. (4)] are given in Fig. 2. The unit of energy in this figure is the j-j splitting Δ of the exciton.

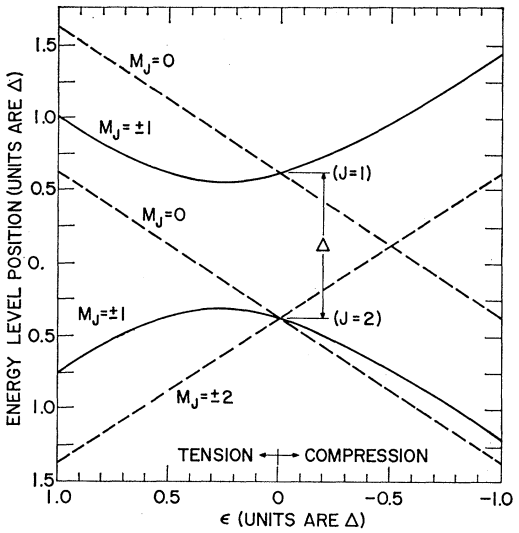

FIG. 2. Splitting of the exciton states under uniaxial stress with the crystal field neglected. The components M_J of angular momentum along the stress axis, which remain good quantum numbers, have been used to label the levels. The unit of energy is Δ, the j-j splitting of the exciton. Center-of-gravity shifts of the exciton are not included in the figure. 2ϵ is the splitting of the valence band maximum with applied uniaxial stress along $\langle 111\rangle$ or $\langle 100\rangle$.

2. *Anisotropic Coupling*

In a cubic crystal the stress or strain coefficients may be anisotropic. This anisotropy has been discussed by Kleiner and Roth,[16] by Thomas,[20] and is greater detail by Picus and Bir,[18] Hasegawa,[21] and Hensel and Feher.[22]

[19] We neglect any coupling to the splitoff $p_{1/2}$ valence band. The spin-orbit splitting has been measured as 82 ± 1 meV by P. J. Dean, G. Kaminsky, and R. B. Zetterstrom, J. Appl. Phys. **38**, 3551 (1967). However, see Ref. 13.

[20] D. G. Thomas, J. Appl. Phys. **32**, 2298 (1961).
[21] H. Hasegawa, Phys. Rev. **129**, 1029 (1963).
[22] J. C. Hensel and G. Feher, Phys. Rev. **129**, 1041 (1963).

For stress along a ⟨100⟩ crystallographic axis the deformation potential is

$$D=D_u, \quad \langle 100\rangle \tag{8a}$$

and hence the stress coefficient is

$$B=(s_{11}-s_{12})D_u, \quad \langle 100\rangle \tag{8b}$$

while for stress along a ⟨111⟩ direction

$$D=D_u', \quad \langle 111\rangle \tag{8c}$$

and B becomes

$$B'=\tfrac{1}{2}s_{44}D_u', \quad \langle 111\rangle. \tag{8d}$$

For other directions of stress the stress field may be resolved into a sum of components along ⟨100⟩ and ⟨111⟩ axes.[11] The strain potential V_s is then the sum of the terms like Eq. (5) computed from these components, or, symbolically,

$$V_s=B\sum \mathcal{T}(100)+B'\sum \mathcal{T}(111), \tag{9a}$$

where we define

$$\mathcal{T}(jkl)=T_{jkl}(20\pi)^{1/2}Y_2^0(\theta), \tag{9b}$$

with $\theta=0$ along the (j,k,l) crystallographic direction. T_{jkl} is the appropriate stress component along that axis, and the sums in (9a) are taken over the three ⟨100⟩ and four ⟨111⟩ directions. This procedure may be shown to be equivalent to use of the effective Hamiltonian of Kleiner and Roth.[16] We note that the stress coefficient B (or deformation potential coefficient D_u), Eqs. (8a) or (8b), relates hole energy to stresses (or strains) which transform as Γ_3 of the T_d group, while B' (or D_u'), Eqs. (8c) or (8d), applies to stresses (or strains) which transform as Γ_5. The former correspond to diagonal and the latter to off-diagonal components of the stress (or strain) tensor expressed in the crystal coordinate system. The effective strain potentials V_s for ⟨100⟩, ⟨111⟩, and ⟨110⟩ stress directions in anisotropic crystals are developed in Appendix B.

On the basis of the theory developed above, the energies and selection rules may be found. For ⟨100⟩ and ⟨111⟩ stress the energies are given by Eqs. (7) with

$$\epsilon=\epsilon_0\equiv B(2F/3) \quad \text{for } F\|\langle 100\rangle, \tag{10a}$$

$$\epsilon=\epsilon_0'\equiv B'(2F/3) \quad \text{for } F\|\langle 111\rangle, \tag{10b}$$

respectively. Only three radiative transitions are allowed. The states with $|M|=1$ (one pair from the higher-energy A line and one pair from the lower-energy B line) emit light polarized perpendicular to the stress (σ polarization) and the state (1,0) (from the A line) emits light polarized parallel to the stress (π polarization). The strength of the emission from the lower state (the B line) is proportional to the square of the amount of the $(1, \pm 1)$ state which its wave function contains. The ratio of the intensities of the B line to the σ component of the A line may be found from the eigenvectors of the matrix Eq. (6),

$$I_{B\sigma}/I_{A\sigma}=\frac{1}{3}\left\{\left[\left(\frac{\Delta}{\epsilon}+1\right)^2+3\right]^{1/2}-\left(\frac{\Delta}{\epsilon}+1\right)\right\}^2 e^{\delta E/kT} \tag{11a}$$

or, for small strain,

$$I_{B\sigma}/I_{A\sigma}=\tfrac{3}{4}(\epsilon/\Delta)^2\, e^{\delta E/kT}, \tag{11b}$$

where δE, the energy difference between the two states, is obtained from Eqs. (7a) and (7d), and the final factor is the Boltzmann factor. Thus, of the five components into which the strain splits the exciton levels, only three appear spectroscopically. The energy levels (relative to the center of gravity E_0) are shown in Fig. 2 as functions of the strain energy ϵ. The dependence of E_0 on stress may be found from the average of the two σ components and the strain energy ϵ from the difference between this energy and the π component. The anisotropy ratio

$$\beta=\epsilon_0'/\epsilon_0 \tag{12}$$

can thus be determined from experiments using ⟨111⟩ and ⟨100⟩ stress.

For a ⟨110⟩ stress in the general case the symmetry is reduced to C_{2v} and the eight exciton states belong in pairs to the four representations Γ_1, Γ_2, Γ_3, and Γ_4.[23] The energies of these states are shown schematically in Fig. 1. The combinations of basis functions which belong to each representation are listed in Table I, and

TABLE I. Exciton basis functions which transform according to the irreducible representations $\Gamma_1-\Gamma_4$ of C_{2v}. The polar (z) axis is taken along the [110] stress and the x axis along the perpendicular [001] direction. All states (including those derived from $J=2$) are odd under reflection, a fact indicated by the minus superscript in the second column.

			C_{2v}
$J=1$	$\|1,0\rangle$	Z	Γ_2
	$\dfrac{\|1,-1\rangle+\|1,1\rangle}{\sqrt{2}}$	Y	Γ_4
	$\dfrac{\|1,-1\rangle-\|1,1\rangle}{\sqrt{2}}$	X	Γ_1
$J=2$	$\|2,0\rangle$	$(3Z^2-R^2)^-$	Γ_3
	$\dfrac{\|2,-1\rangle+\|2,1\rangle}{\sqrt{2}}$	$(XZ)^-$	Γ_4
	$\dfrac{\|2,-1\rangle-\|2,1\rangle}{\sqrt{2}}$	$(ZY)^-$	Γ_1
	$\dfrac{\|2,-2\rangle+\|2,2\rangle}{\sqrt{2}}$	$(X^2-Y^2)^-$	Γ_3
	$\dfrac{\|2,-2\rangle-\|2,2\rangle}{\sqrt{2}}$	$(XY)^-$	Γ_2

[23] For this case, if we include the inversion symmetry, no new information is obtained. The group becomes D_{2h}, and the representations become Γ_3^-, Γ_4^-, Γ_1^-, and Γ_3^-, respectively.

their energies and wave functions are derived in Appendix B.

We find for ⟨110⟩ stress in an anisotropic cubic material that six spectral lines can appear—two σ components, Γ_1 and Γ_4, from the A line and two from the B line, and also a π component, Γ_2, from each. The two Γ_3 components remain forbidden. The energies $E_i^{\pm}$ of these lines are shown versus hole energy ϵ_0'', Eq. (B20), in Fig. 3 for the anisotropy ratio, $\beta=2$. The energy E_2 and the intensity ratio A_2^2 (omitting the Boltzmann factor) are shown versus stress in Fig. 12. This intensity ratio $I_{B\pi}/I_{A\pi}=A_2^2$ for the two $\Gamma_2(\pi)$ components is very sensitive to the anisotropy, since it vanishes for $\beta=1$ but for $\beta\neq1$ reaches unity at the small value of stress, where

$$3\epsilon_0'+\epsilon_0=2\Delta. \tag{13}$$

This fact provides a sensitive check of the consistency of this model with the experimental results.

The appearance of the crystal-field splitting introduces small corrections into the energy expressions derived above. In particular, for strain energies small compared to the $\Gamma_3-\Gamma_4$ separation of $\sim$0.3 meV the slopes $dE/d\epsilon_0$ are changed. These initial slopes for the levels which arise from the Γ_3 and Γ_4 states are listed in Table II together with the expected polarizations. As the strain energy rises above the zero stress splitting the levels rapidly approach those calculated in the absence of the crystal field (See Fig. 1).

TABLE II. Initial slopes $dE/d\epsilon$ and polarizations P at small strain energy ϵ for the Γ_3 and Γ_4 levels split from the $J=2$ state by coupling to the crystal. The rows labeled IR list the irreducible representations under the appropriate groups. σ_x indicates polarization along the ⟨001⟩ direction perpendicular to the ⟨110⟩ stress.

Group		D_{2d}		C_{3v}		C_{2v}		
Stress	T_d	⟨100⟩		⟨111⟩		⟨110⟩		
IR	Γ_3	Γ_1	Γ_3	Γ_3		Γ_1	Γ_3	
P	···	···	···	σ		σ_x	···	
Slope	···	−1	1	0		−0.5	0.5	
IR	Γ_4	Γ_2	Γ_5	Γ_2	Γ_3	Γ_2	Γ_3	Γ_4
P	···	···	σ	···	σ	π	···	σ_y
Slope	···	1	−0.5	−1	0.5	1	−0.5	−0.5

IV. EXPERIMENTAL RESULTS

A. Zero-Stress Spectra

Photoluminescence spectra of bismuth-doped GaP in the region of zero-phonon emission from the Bi exciton are shown in Fig. 4. Curves A and B were excited with focused 5145 Å light and curve C with 4880 Å light from an argon ion laser. The temperatures of the ambient in the Dewar were 11° and 1.8° as indicated in the figure. Curve A, taken at the higher temperature clearly shows the A line produced by the allowed $J=1$ to $J=0$ dipole transition. No lines appear in curve B, since at the lower temperature only the low-

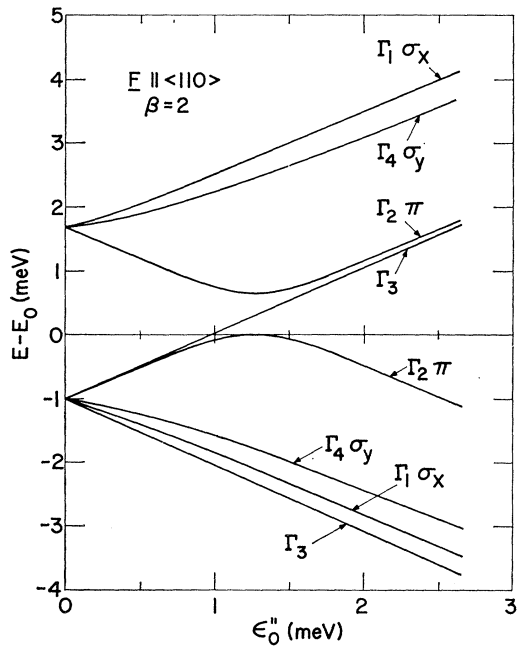

FIG. 3. Splitting of the exciton states under ⟨110⟩ uniaxial stress for an anisotropic crystal, $\beta=2$, with the crystal field neglected. The representations of the C_{2v} group and the polarization of the emitted radiation are indicated for each level (see Table I). The energies are in meV for the Bi exciton in GaP. σ_x represents the component observable with electric vector, $\mathbf{E}$, perpendicular to the stress direction when the light propagation direction $\mathbf{q}$ is along $[1\bar{1}0]$; σ_y is observable with $\mathbf{E}\perp\mathbf{F}$ when $\mathbf{q}\|[001]$.

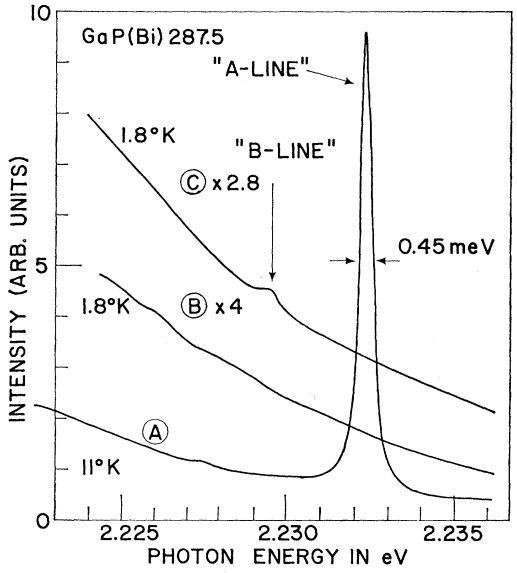

FIG. 4. The photoluminescence spectrum of excitons bound to Bi in GaP at 1.8 and 11°K in the region of the no-phonon transitions: lines A and B. The approximate spectral resolution for measurements using the monochromator is given by the half-width of the zero-stress A line. The traces denoted by the encircled letters A and B are taken using the 5145 Å line of the argon laser as the exciting radiation; for curve C the 4880 Å line was used.

energy $J=2$ state is populated and dipole transitions from it to the ground state are forbidden. The transition from the $J=2$ state to the ground state, the B line, can be observed if the selection rules are relaxed by an appropriate perturbation applied to the crystal. This is accomplished in curve C, where the inhomogeneous absorption of the higher energy 4880 Å laser light near the crystal surface generated the necessary perturbation. The changes produced in these spectra by the application of uniaxial stress are described in Sec. IV B.

B. Spectra Produced under Uniaxial Stress

Photoluminescence spectra from Bi excitons in GaP under uniaxial compression are shown in Fig. 5, Fig. 7, and Figs. 9 and 10 for stress applied along the ⟨111⟩, ⟨100⟩, and ⟨110⟩ axes, respectively. The energies of the emission lines are shown as functions of the applied stress in Figs. 6, 8, and 11. Two features are common to all three directions:

(1) The A line splits into two components with the lower energy branch, $A2$, polarized predominantly parallel (π) and the higher, $A1$, perpendicular (σ) to the stress direction. The higher branch, $A1$, is noticeably broader than $A2$.

(2) With increasing stress the B line appears with increasing intensity and exhibits a prominent component polarized perpendicular to the stress direction which shifts with stress nearly parallel to the lower A line component $A2$.

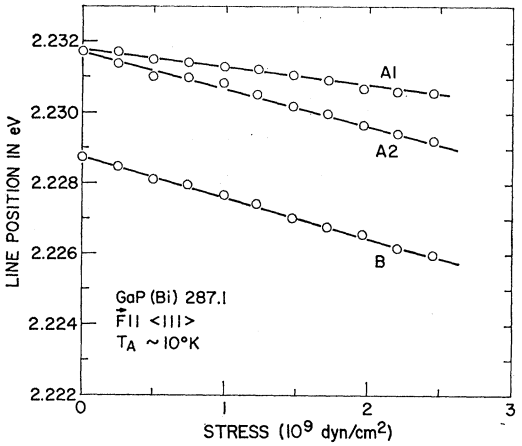

FIG. 6. The stress dependence of the A and B exciton recombination lines with the stress along the ⟨111⟩ crystallographic direction. Data taken with the sample in an ambient at about 10°K are shown.

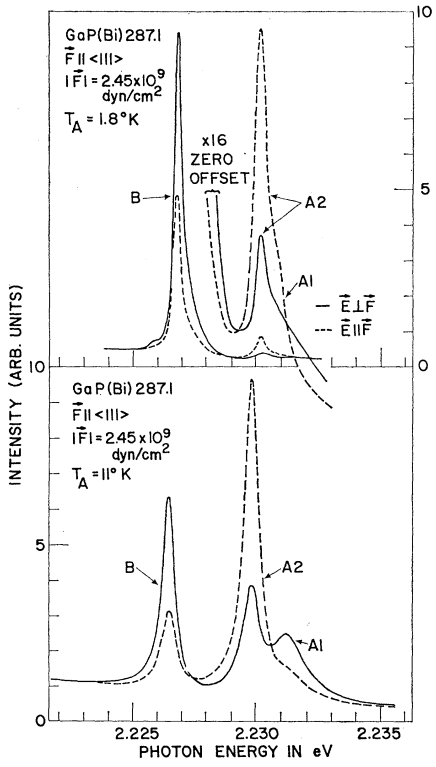

FIG. 5. The effect of a compressive stress along the ⟨111⟩ crystallographic direction on the zero phonon exciton recombination spectrum of GaP(Bi). The upper half of the figure shows the spectrum with the sample in an ambient of 1.8°K; the lower, about 11°K. The emission observed with polarization parallel and perpendicular to the stress axis is shown by dashed and solid lines, respectively. In commonly used units 1 (dyn/cm²) ≡ 1.02×10^{-6} (kg/cm²).

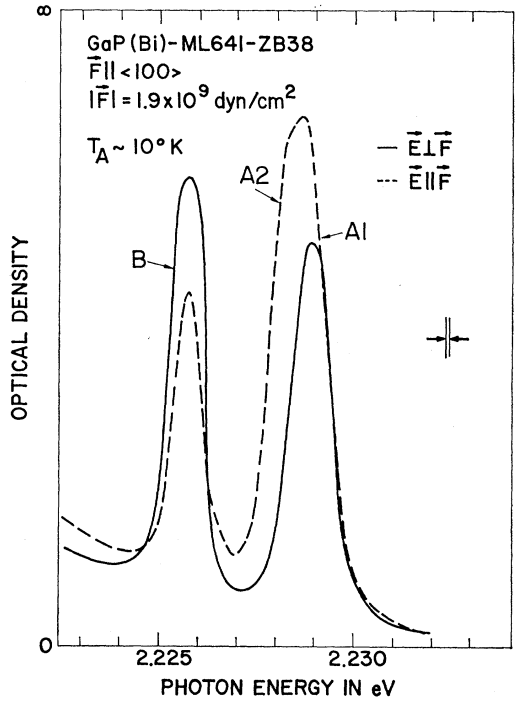

FIG. 7. The effect of a ⟨100⟩ compressive stress on the recombination spectrum of the exciton bound to Bi in GaP. The spectrum was taken with the sample in an ambient at about 10°K. The relative intensities of the lines observed in the two polarizations are approximate. The spectrum shown is a densitometer trace of a photographic plate.

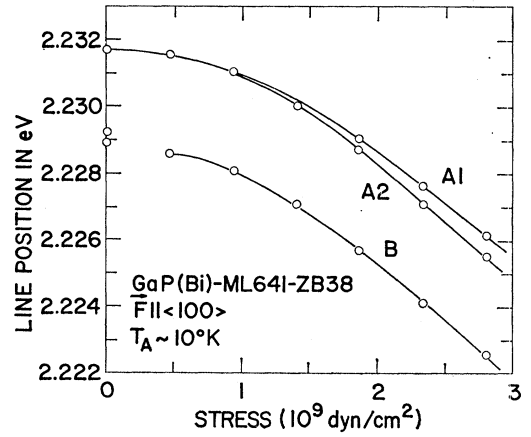

FIG. 8. The stress dependence of the A and B Bi exciton recombination lines with the stress along the ⟨100⟩ crystallographic direction. Data taken with the sample in an ambient at about 10°K are shown.

In addition to the above similarities in the spectra there are several features which serve to distinguish the spectra according to the direction of the applied stress.

(1) Under ⟨110⟩ stress, Figs. 9–11, the B line exhibits multiple components. Most pronounced is a doublet $B2$ and $B3$ polarized predominantly perpendicular to the stress (though $B3$ is less strongly polarized than is

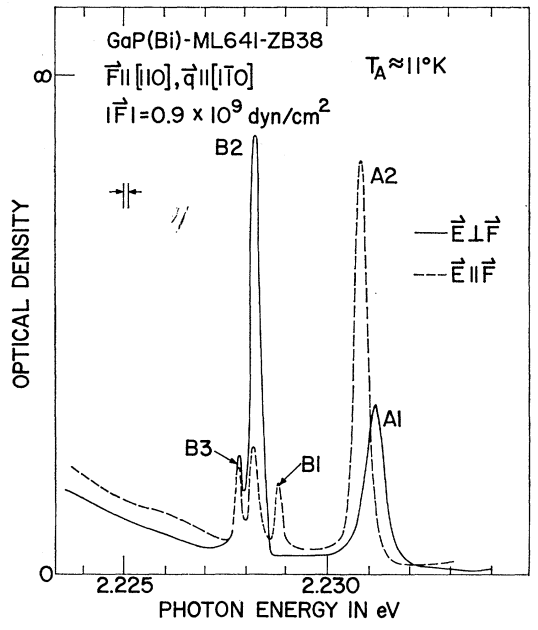

FIG. 9. The effect of a compressive stress of 0.9×10^9 dyn/cm^2 along [110] on the recombination spectrum of the exciton bound to Bi in GaP. Light emitted with the propagation vector $\mathbf{q}$ along [1$\bar{1}$0] is recorded here. This spectrum is a densitometer trace of a spectrographic plate. The spectral resolution for the measurement is indicated in the figure. The relative intensities of the lines in the two polarizations are approximate.

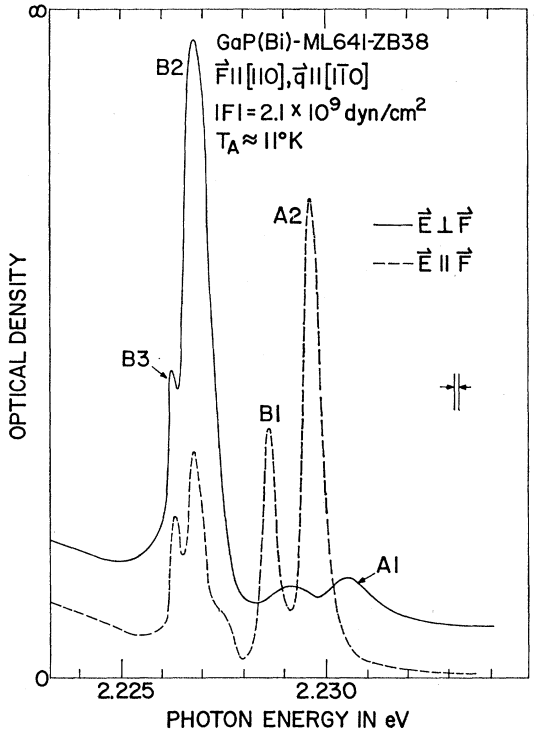

FIG. 10. The effect of a compressive stress of 2.1 $\times10^9$ dyn/cm^2 along [110] on the recombination spectrum of the exciton bound to Bi in GaP. Light emitted with the propagation vector $\mathbf{q}$ along [1$\bar{1}$0] is recorded here. This spectrum is a densitometer trace of a spectrographic plate. The spectral resolution for the measurement is indicated in the figure. The relative intensities of the lines in the two polarizations are approximate.

$B2$) which maintains a nearly constant separation of ~0.4 to 0.5 meV over most of the range of stresses used. At zero stress the B line is seen as a very weak doublet with a splitting of 0.25 meV. In addition, a parallel polarized component $B1$ appears and ap-

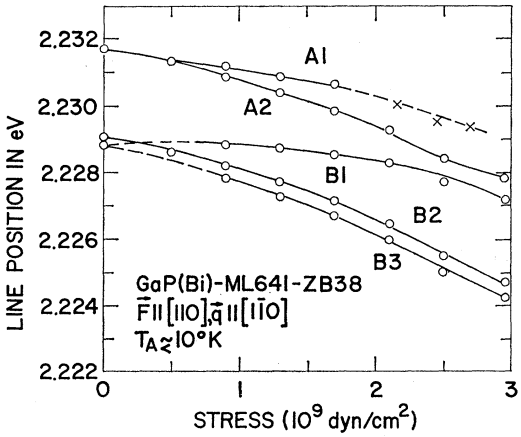

FIG. 11. The stress dependence of the A and B Bi exciton recombination lines with stress along the ⟨110⟩ crystallographic direction. Part of the data for component $A1$, not observable at the temperature of this measurement, has been introduced from another measurement and is indicated by x's.

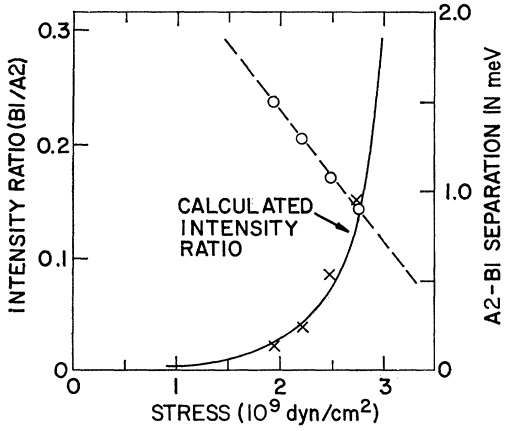

FIG. 12. Comparison of the expected intensity ratio of the components $B1/A2$ in the polarization with the electric vector parallel to the stress axis (solid line) with the experimentally observed intensity ratio (x's) as a function of the magnitude of the applied stress along [110]. The experimental data have been adjusted by the Boltzmann factor. The anisotropy ratio β is assumed to be 2 in this calculation. The experimental (0's) and theoretical (dashed line) energy spacing between $A2$ and $B1$ is also shown.

proaches but does not cross the parallel A line component $A2$ at large stress. The intensity of this component is shown as a function of stress in Fig. 12. The doublet $B2$ and $B3$ occasionally appeared weakly in samples of other orientation at zero stress but became unresolvable as the stress was increased.

(2) The $A1$-$A2$ separations are strongly anisotropic, being approximately 2.5 times larger for ⟨111⟩ than for ⟨100⟩ stress and intermediate for ⟨110⟩ stress.

(3) The center of gravity of the lines shows a gradual decrease approximately linear in stress for ⟨111⟩ stress but shows a much more rapid quadratic decrease for ⟨100⟩ stress. Again the ⟨110⟩ case is intermediate.

In all of these spectra the polarization is found to be mixed to some extent, although always one direction—that predicted theoretically—dominates. It was found that this polarization mixing was due to scattering at the sample surface and could be eliminated in a large sample whose surfaces had been polished prior to etching. Reasonably narrow lines, $\lesssim 0.5$ meV, were obtained in all spectra except those under ⟨100⟩ stress, Fig. 7. For this orientation the stress inhomogeneities in the sample, amplified by the large center-of-gravity shifts of the lines, produced linewidths of over 1 meV. In the following section these results are interpreted in terms of the theoretical model developed in Sec. III.

V. DISCUSSION

We interpret the experimental results in terms of three major consequences of the applied stress: a uniform shift of the levels due to the hydrostatic-stress component and the effects of the shear stress on the electron and hole states.

A. Hydrostatic Stress

The hydrostatic component ($\frac{1}{3}F$) of the stress produces a uniform shift of the levels as described by Eq. (2) of Sec. III. This term is isotropic with respect to the direction of the uniaxial stress and is given experimentally by the center-of-gravity shift of the exciton energy with $F\|\langle 111\rangle$, Fig. 6. It is plotted against stress as the upper curve in Fig. 14(a). From its slope and the compliance coefficients[24] listed in Eq. (16) we can compute the sum of the deformation potentials appearing in Eq. (2),

$$\Xi_d + D_d^v + \tfrac{1}{3}\Xi_u = 1.5 \pm 0.2 \text{ eV}. \quad (14a)$$

This is less than one-half of the value obtained by Balslev for free excitons in GaP,[25]

$$\Xi_d + D_d^v + \tfrac{1}{3}\Xi_u = 3.7 \pm 0.6 \text{ eV}, \quad (14b)$$

but is larger by 50% than the value reported by Zallen and Paul[26] for the band gap,

$$\tfrac{1}{3}(dE_g/dP)/(s_{11}+2s_{12}) = 1.0 \text{ eV} \pm 10\%. \quad (14c)$$

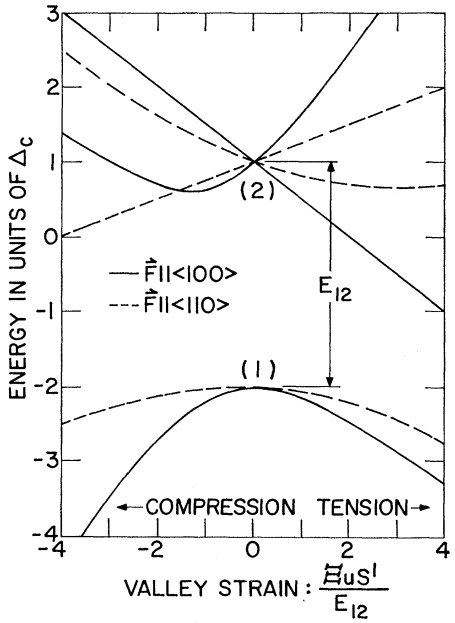

FIG. 13. The effect of uniaxial stress in the ⟨110⟩ and ⟨100⟩ crystallographic directions on the ground state of the bound exciton in GaP. The j-j interaction has been set to zero, and shifts due to the hydrostatic component of the stress have not been shown. The zero of energy denotes the center of gravity of the levels. The conduction-band minima have been assumed to lie at the Brillouin-zone boundary along the ⟨100⟩ axes. The figure is for the case where the valley orbit splitting lowers the energy of the singlet electron state. The effect of a ⟨111⟩ uniaxial stress can be represented by horizontal lines through the zero stress positions in the figure. $E_{12}=3\Delta_c$ is the valley orbit splitting, Ξ_u is the conduction band shear deformation potential, and $s'=2(s_{11}-s_{12})T$ for ⟨100⟩ stress and half this value for ⟨110⟩ stress.

[24] R. Weil and W. O. Groves, J. Appl. Phys. **39**, 4049 (1968).
[25] I. Balslev, J. Phys. Soc. Japan Suppl. **21**, 101 (1966). The measured values of s_{ij} from Ref. 24 have been used to correct the deformation potentials reported here.
[26] R. Zallen and W. Paul, Phys. Rev. **134**, A1628 (1964).

A difference between these deformation potentials for bound and free excitons could be due to a combination of two effects. (1) The localization of the exciton wave function near the Bi core could produce a change in the deformation potentials because of the different nature of the wave function in the central cell. (2) The compliance coefficient ($s_{11}+2s_{12}$) which appears in Eq. (2) may be changed by the distortion of the crystal around the large Bi impurity. Use of the bulk value to obtain (14a) would then yield an erroneous result.

B. Valley-Orbit Splitting of Exciton

Axial stress in any direction other than ⟨111⟩ lifts the degeneracy of the ⟨100⟩ conduction-band valleys and shifts the energy of the valley-orbit split states. This anisotropic shift is in general nonlinear because of mixing among the three valleys and appears as a center of gravity shift of the lower-lying exciton levels. The theory is described in Appendix A, and the stress dependence of this part of the exciton energy is shown in Fig. 13 for stresses in ⟨100⟩ and ⟨110⟩ directions. The figure represents the normal case for which the interaction lowers the energy of the singlet state (as found for the Bi exciton). The same figure viewed upside down with the signs of both scales changed represents solutions for the inverted case in which the doublet state lies lower. Using Balslev's estimate of the value of Ξ_u,[25]

$$\Xi_u = 6.9 \text{ eV},$$

and the compliance coefficients listed in Eq. (16), we estimate that the maximum valley strain energy attained in our experiments was

$$\Xi_u s'/E_{12} = -1.2.$$

Values of the center-of-gravity energy of the exciton are shown versus stress in Fig. 14(a) for ⟨111⟩, ⟨110⟩, and ⟨100⟩ stresses. These have been deduced from the energies of the two visible components $A1$ and $A2$,

$$E_0 = \tfrac{1}{3}(2E_{A\sigma}+E_{A\pi}) - 5\Delta/8. \quad (15)$$

A small correction for mixing of $A1$ and B was computed from Fig. 2 and applied to the data, although it was found to be smaller than the experimental uncertainty of the points. The three curves exhibit the hydrostatic pressure shift alone for ⟨111⟩ stress and the sum of this and the shear contribution shown in Fig. 13 for ⟨110⟩ and ⟨100⟩ stress. The near tangency of the three curves at zero stress and their widely differing values at large stress clearly demonstrate that the electron states are derived from the symmetric valley-orbit combination of the ⟨100⟩ conduction-band minima.

The ⟨100⟩ curve with the ⟨111⟩ hydrostatic part subtracted is redrawn in Fig. 14(b) and compared with three theoretical curves scaled from Fig. 13 for $E_{12}=24$, 30, and 36 meV and matched at the largest stress.

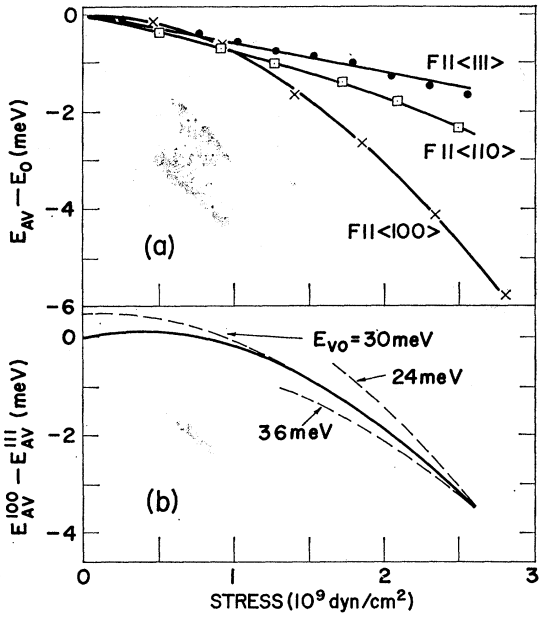

FIG. 14. (a) Center of gravity of the exciton bound to Bi in GaP as a function of stress magnitude with the stress along either the ⟨111⟩, ⟨100⟩, or ⟨110⟩ crystallographic direction. The curves shown have been calculated from the experimentally observed stress dependence of the components $A1$ and $A2$ with the stress induced interaction with the B line taken into account. (b) The difference between the centers of gravity of the exciton with the stress along ⟨100⟩ and ⟨111⟩ is shown by the solid line as a function of stress magnitude. The dashed curves represent the theoretically expected stress dependence of the same quantity calculated for valley orbit splittings of 24, 30, and 36 meV.

Although there are qualitative differences at small stress, the experimental curve at large stress agrees with the theoretical curve having a valley-orbit splitting of

$$E_{12} = 30 \text{ meV}.$$

We estimate that the uncertainty is about ±10 meV. The uncertainty in the data arises chiefly from stress inhomogeneities which became apparent at the larger stresses in the small samples available. (In fact, it was this inhomogeneity which determined the largest stresses used.) For small stresses, however, we believe that the discrepancies between theory and experiment—in particular the initial rise of the experimental curve in Fig. 14(b)—lie outside of the experimental uncertainties and are due to coupling of the three-valley conduction band to E-type lattice distortions as discussed in Sec. III B. At large stress where the splitting of the exciton levels reduces the effectiveness of the vibronic coupling, the data approach the curve predicted by the simple theory.[27]

C. Effects of Stress on Hole States

The remaining effects of stress on the exciton energies arise from perturbation of the hole states through the

[27] P. Price, Phys. Rev. **104**, 1223 (1956).

shear-deformation potentials D_u and D_u' (or the stress coefficients B and B'). The predicted behavior, which is shown in Fig. 2 for $\langle 111\rangle$ and $\langle 100\rangle$ stresses and in Fig. 3 for $\langle 110\rangle$ stress with $B'/B=2$, represents the observed stress dependence qualitatively quite well. Even the component $B1$ is observed only with $F\|\langle 110\rangle$ as predicted, and its intensity is adequately represented by calculations based on the j-j coupling model of the exciton, Fig. 12. Although these results corroborate the essential features of the model, some distinct differences between the observed and calculated results are evident. Some of these can be explained in terms of the crystal field splitting, though others cannot.

(1) The appearance of the doublet $B2$ and $B3$ for $F\|\langle 110\rangle$ is clear evidence for a "crystal-field" splitting of ~ 0.25 meV between the Γ_3 and Γ_4 sublevels of the $J=2$ exciton. For the crystal geometry of Fig. 11 with the light propagating along the $[1\bar{1}0]$ direction perpendicular to the [110] stress axis, emission from the Γ_1 level (see Fig. 3) should be allowed and strongly polarized in the [001] direction perpendicular to the stress. Emission from the Γ_4 component, although allowed by symmetry, could produce light propagating in the direction observed only after undergoing scattering within the crystal and would hence be largely unpolarized. This allows us to identify the weaker and less strongly polarized component $B3$ with the Γ_4 level (of C_{2v}) and the higher-energy component $B2$ with the Γ_1 level. Hence we conclude that the doublet Γ_3 state of the unperturbed T_d crystal lies above the triplet Γ_4 state—see Table II. This is in agreement with the conclusions of Ref. 28. The stress-dependent separation between the Γ_1 and Γ_4 levels (of C_{2v}) shown in Fig. 3 is apparently too small to be resolved with this geometry at the stresses used.

(2) The difference between the energies of lines $A2$ and B was found to be nearly independent of stress along $\langle 100\rangle$ (Fig. 8), and to increase slightly with increasing stress along $\langle 111\rangle$ (Fig. 6), although according to our model, Fig. 2, the initial slopes should have differed by a factor of two and produced a decrease in the separation $A2$-B for both orientations. The increase in Fig. 6 was $\sim 10\%$ of the $A1$-$A2$ splitting. A careful study of the energies and selection rules of the states under stress reveals that this discrepancy cannot be explained by inclusion of the crystal-field splitting. This anomalous result can be produced, however, if the effective deformation potential for splitting of the $J=1$ levels which generate the A lines is smaller by a factor of ~ 2.2 than that for the $J=2$ levels and the B lines. Indeed, the data of Fig. 11 confirm this approximate ratio for the deformation potentials, since the splitting between $B1$ and $B3$ at small stress is somewhat greater than twice the $A1$-$A2$ splitting, and interactions between the levels can account for only a small part of the difference.

(3) Knowledge of the splitting of the exciton states under stress allows us to determine the deformation potentials D_u and D_u' of the holes and the anisotropy ratio β. Using the elastic compliance coefficients of GaP determined by Weil and Groves,[24]

$$\begin{aligned} s_{11}&=0.973\times 10^{-12}\ \text{cm}^2/\text{dyn}\pm 0.97\%,\\ s_{12}&=-0.299\times 10^{-12}\ \text{cm}^2/\text{dyn}\pm 1.8\%,\\ s_{44}&=1.419\times 10^{-12}\ \text{cm}^2/\text{dyn}\pm 0.24\%, \end{aligned} \tag{16}$$

and making small corrections for interactions among the exciton states—see Eqs. (7) and Fig. 2—we find the following deformation potentials for the $J=1$ levels of the Bi excitons:

$$D_u=0.17\pm 0.05\ \text{eV},\quad (A\ \text{line}) \tag{17a}$$

$$D_u'=0.77\pm 0.05\ \text{eV},\quad (A\ \text{line}) \tag{17b}$$

and for the $J=2$ levels about twice these values,

$$D_u=0.34\ \text{eV},\quad (B\ \text{line}) \tag{17c}$$

$$D_u'=1.7\ \text{eV},\quad (B\ \text{line}). \tag{17d}$$

These are significantly smaller than the deformation potentials determined by Balslev for free excitons,[25]

$$D_u=2.2\pm 0.2\ \text{eV}, \tag{18a}$$

$$D_u'=3.9\pm 0.4\ \text{eV}. \tag{18b}$$

In addition, the anisotropy ratio, Eq. (12), is found to be

$$\beta=2.5, \tag{19}$$

although it is nearly 1.0 for free excitons.

As discussed in Sec. III B many of the above differences between the observed results and those predicted by the simple model may be a consequence of the vibronic coupling between the exciton and the lattice. However, two additional effects may also account in part for the observed discrepancies. (1) The changes in the effective masses of the two branches of the valence band which occur as the bands separate under stress cause changes in the binding energies of the corresponding bound-hole states and reduce their effective deformation potentials. This effect has been considered by Price[29] and calculated by Bir, Butikov, and Pikus[30,31] for effective mass acceptors in Ge and Si. The latter authors find that the effective deformation potentials for bound holes in Ge are reduced by about 40% and those in Si by 10%. For both materials the anisotropy

[28] Studies of the Zeeman effect of Bi excitons in GaP by B. Welber [Phys. Letters **29A**, 401 (1969)] and P. J. Dean and R. A. Faulkner [Phys. Rev. **185**, 1064 (1969)] give results consistent with the j-j coupling of the ($J=2$) exciton also found here.

[29] P. Price, Phys. Rev. **124**, 713 (1961).

[30] G. E. Pikus and G. L. Bir, Phys. Rev. Letters **6**, 103 (1961).

[31] G. L. Bir, E. I. Butikov, and G. E. Pikus, J. Phys. Chem. Solids **24**, 1467 (1963).

ratio β is increased by about 10%. In more tightly bound states the admixture of band states farther from $k=0$ may enhance the magnitude of this effect. (2) The distortion of the lattice near the impurity caused by the mismatch between the size of the Bi and the P atom it replaces may decrease anisotropically the compliance coefficients which relate the stress to the local strain it produces. A correction for this effect could increase the size of the deformation potentials we calculate, Eqs. (17), but seems unlikely to explain the large discrepancies observed.

VI. SUMMARY

The effects of uniaxial compression on zero-phonon emission from excitons bound to Bi impurities in GaP have been studied by photoluminescence at liquid helium temperatures. The samples were illuminated with either the 4880 or 5145 Å line of an argon ion laser. Data taken with uniaxial stress applied along the ⟨111⟩, ⟨100⟩, and ⟨110⟩ crystallographic directions confirm that the electron part of the exciton wave function is a symmetric combination of the ⟨100⟩ conduction-band valleys. A valley-orbit splitting of 30 ± 10 meV is estimated. The behavior of the exciton states with applied uniaxial stress is qualitatively consistent with the simple j-j coupling model for the exciton. A crystal-field splitting of the B line into two components separated by approximately 0.25 meV is noted in agreement with Welber[28] and Dean and Faulkner.[28] The shear deformation potentials of the holes, given in Eq. (17), are found to be considerably smaller than those characterizing band states and to be twice as large for the $J=2$ state (the B line) as for the $J=1$ state (the A line). The anisotropy ratio β is found to be ~2.5 times the free exciton value of 1.0. An interpretation of these anomalous results is suggested in terms of the dynamic Jahn-Teller effect.

ACKNOWLEDGMENT

It is a pleasure to thank Dr. L. M. Foster and J. E. Scardefield for making available the bismuth-doped GaP from which most of the experimental data were obtained. We are grateful to Dr. M. R. Lorenz for providing the sample with an epitaxial bismuth-doped-solution overgrowth. Helpful discussions with Dr. Jane van W. Morgan concerning the theory of stress effects on exciton states are gratefully acknowledged.

APPENDIX A

The theory of the valley-orbit interaction is given in Ref. 8, and the effects of stress are described by Price[27] and by Wilson and Feher.[32] For a three valley conduction band the valley-orbit matrix with strain in either a ⟨100⟩ or ⟨110⟩ direction is

$$H_{v0}=-\Delta_c\begin{bmatrix}-2x & 1 & 1\\ 1 & x & 1\\ 1 & 1 & x\end{bmatrix}, \tag{A1}$$

where Δ_c is the interaction energy connecting two valleys and x is the "valley strain" energy,

$$x=\Xi_u s'/3\Delta_c. \tag{A2}$$

The valley-orbit splitting between the singlet and doublet at zero stress is

$$E_{12}=3\Delta_c \tag{A3}$$

and the effective shear strain for a ⟨100⟩ stress is[32]

$$s'=2(s_{11}-s_{12})T, \quad \langle100\rangle. \tag{A4}$$

For ⟨110⟩ stress s' is changed in sign and reduced by a factor of 2,

$$s'=-(s_{11}-s_{12})T, \quad \langle110\rangle. \tag{A5}$$

The energies derived from Eq. (A1) with $\Delta_c>0$ (the "normal" case) are shown as functions of x in Fig. 13 for both ⟨100⟩ and ⟨110⟩ stress. For ⟨111⟩ stress the "valley strain" s' is zero.

APPENDIX B

We wish to calculate the exciton wave functions and energies when stress is applied in the ⟨100⟩, ⟨111⟩, and ⟨110⟩ directions in an anisotropic cubic crystal. We shall use Eq. (9a) with the notation of Eqs. (9b), (8), and (10).

If the splitting is stress-isotropic, we have

$$\beta=B'/B=1,$$

V_s in (9a) has the same (axial) symmetry as the stress,[20–22] and the energies are given by Eqs. (7). For the general case, $\beta\neq1$, the symmetry of V_s depends upon the orientation of the stress in the crystal. For stress along ⟨100⟩ or ⟨111⟩ axes V_s has the same symmetry (Y_2^0) as the stress,[21] see Fig. 1. For the former,

$$V_s=B\mathcal{T}(100), \tag{B1}$$

while for the latter

$$V_s=B'\mathcal{T}(111). \tag{B2}$$

A compressive stress field along the [110] direction may be resolved into three components—one (tension) component along the perpendicular [001] axis, which belongs to Γ_3 (in T_d), and two (compressive) components along the adjacent ⟨111⟩ directions, [111] and [11$\bar{1}$], which belong to Γ_5. If $B=B'$, these three terms recombine to form a single Y_2^0 effective potential along the stress direction. When $B\neq B'$, we add to and subtract from V_s a term equal to B' times the component $\mathbf{T}(001)$ along the [001] axis. Thus the total strain potential reduces to

$$V_s=B'\mathcal{T}(110)+\delta B\mathcal{T}(001) \tag{B3}$$

[32] D. K. Wilson and G. Feher, Phys. Rev. **124**, 1068 (1961).

or relative to the [110] axis

$$V_s=-(20\pi)^{1/2}(\tfrac{2}{3}F)[(B'+\delta B/4)Y_2^0 -(\tfrac{1}{4}\delta B\sqrt{3})(Y_2^2+Y_2^{-2})/\sqrt{2}], \quad \text{(B4)}$$

where $\mathcal{T}(110)$ is the total uniaxial stress field oriented along [110], and we have used $\delta B=B-B'$. The sum of the terms multiplied by δB in Eq. (B4) transforms as Y_2^0 about [001] but possesses off-diagonal matrix elements between the $|m|=\frac{3}{2}$ and the $|m|=\frac{1}{2}$ hole states quantized along [110]. The resulting matrix for these latter states is the same as Eq. (23) of Hensel and Feher[22] and can be diagonalized to give the effective stress coefficient B'' and the mixing of the hole states. Thus

$$B''=\tfrac{1}{2}(B^2+3B'^2)^{1/2}, \quad \text{(B5)}$$

as quoted by Thomas.[20] We now diagonalize the strain matrix generated by the potential V_s of Eq. (B4).

We choose a set of axes such that the z axis coincides with the [110] stress direction, the x axis lies along the perpendicular [001] axis and coincides with the C_2 axis of the group, and the y axis lies in the [1$\bar{1}$0] direction. The basis functions of the $J=1$ and $J=2$ states belong to D_1^- and D_2^-, respectively. The combinations of these functions which belong to the representations of C_{2v} are listed in Table I. The nonaxial part of the strain potential (B4) mixes the pairs of states within each representation. The resulting 2×2 matrices M_i, their eigenvalues $E_i^{\pm}$ (relative to E_0), and A_i the amount of admixture of the $J=1$ (or $M=0$ for Γ_3) basis states into the lower-lying eigenstates are given below for the four representations Γ_i, $i=1$–4. The definition of A_i is such that the wave functions of the lower states are

$$\Psi_i^-=(1+|A_i|^2)^{-1/2}[\Psi_i(J=2)+A_i\Psi_i(J=1)], \quad i=1, 2, 4 \quad \text{(B6)}$$

and

$$\Psi_3^-=(1+|A_3|^2)^{-1/2}[\Psi_3(M=0)+A_3\Psi_3(M=2)]. \quad \text{(B7)}$$

We set $\epsilon_0-\epsilon_0'=\delta\epsilon_0$ with ϵ_0 and ϵ_0' defined by Eqs. (10). Thus, for Γ_1,

$$\mathbf{M}_1=\begin{bmatrix}\frac{5}{8}\Delta+\frac{1}{2}\epsilon_0'-\frac{1}{4}\delta\epsilon_0 & \frac{1}{2}\sqrt{3}(\epsilon_0'+\frac{1}{2}\delta\epsilon_0)\\ \frac{1}{2}\sqrt{3}(\epsilon_0'+\frac{1}{2}\delta\epsilon_0) & -\frac{3}{8}\Delta-\frac{1}{2}\epsilon_0'+\frac{1}{4}\delta\epsilon_0\end{bmatrix}, \quad \text{(B8)}$$

$$E_1^{\pm}=\tfrac{1}{8}\Delta\pm\tfrac{1}{2}\{(\Delta+\epsilon_0'-\tfrac{1}{2}\delta\epsilon_0)^2+3(\epsilon_0'+\tfrac{1}{2}\delta\epsilon_0)^2\}^{1/2}, \quad \text{(B9)}$$

and

$$A_1=(2/\sqrt{3})(E_1^+-\tfrac{5}{8}\Delta-\tfrac{1}{2}\epsilon_0'+\tfrac{1}{4}\delta\epsilon_0)/(\epsilon_0'+\tfrac{1}{2}\delta\epsilon_0). \quad \text{(B10)}$$

For Γ_2,

$$\mathbf{M}_2=\begin{bmatrix}\frac{5}{8}\Delta-\epsilon_0'-\frac{1}{4}\delta\epsilon_0 & \frac{1}{4}\sqrt{3}\delta\epsilon_0\\ \frac{1}{4}\sqrt{3}\delta\epsilon_0 & -\frac{3}{8}\Delta+\epsilon_0'+\frac{1}{4}\delta\epsilon_0\end{bmatrix}, \quad \text{(B11)}$$

$$E_2^{\pm}=\tfrac{1}{8}\Delta\pm\tfrac{1}{2}[(\Delta-2\epsilon_0'-\tfrac{1}{2}\delta\epsilon_0)^2+\tfrac{3}{4}\delta\epsilon_0^2]^{1/2}, \quad \text{(B12)}$$

and

$$A_2=(4/\sqrt{3})(E_2^+-\tfrac{5}{8}\Delta+\epsilon_0'+\tfrac{1}{4}\delta\epsilon_0)/\delta\epsilon_0. \quad \text{(B13)}$$

For Γ_3,

$$\mathbf{M}_3=\begin{bmatrix}-\frac{3}{8}\Delta-\epsilon_0'-\frac{1}{4}\delta\epsilon_0 & -\frac{1}{4}\sqrt{3}\delta\epsilon_0\\ -\frac{1}{4}\sqrt{3}\delta\epsilon_0 & -\frac{3}{8}\Delta+\epsilon_0'+\frac{1}{4}\delta\epsilon_0\end{bmatrix}, \quad \text{(B14)}$$

$$E_3^{\pm}=-\tfrac{3}{8}\Delta\pm[(\epsilon_0'+\tfrac{1}{4}\delta\epsilon_0)^2+\tfrac{3}{16}\delta\epsilon_0^2]^{1/2}, \quad \text{(B15)}$$

and

$$A_3=-(4/\sqrt{3})(E_3^++\tfrac{3}{8}\Delta-\epsilon_0'+\tfrac{1}{4}\delta\epsilon_0)/\delta\epsilon_0. \quad \text{(B16)}$$

For Γ_4,

$$\mathbf{M}_4=\begin{bmatrix}\frac{5}{8}\Delta+\frac{1}{2}(\epsilon_0'+\delta\epsilon_0) & \frac{1}{2}\sqrt{3}\epsilon_0'\\ \frac{1}{2}\sqrt{3}\epsilon_0' & -\frac{3}{8}\Delta-\frac{1}{2}(\epsilon_0'+\delta\epsilon_0)\end{bmatrix}, \quad \text{(B17)}$$

$$E_4^{\pm}=\tfrac{1}{8}\Delta\pm\tfrac{1}{2}[(\Delta+\epsilon_0'+\delta\epsilon_0)^2+3\epsilon_0'^2]^{1/2}, \quad \text{(B18)}$$

and

$$A_4=(2/\sqrt{3})(E_4^+-\tfrac{5}{8}\Delta-\tfrac{1}{2}\epsilon_0'-\tfrac{1}{2}\delta\epsilon_0)/\epsilon_0'. \quad \text{(B19)}$$

We note that since both Γ_3 states emerge from the $J=2$ manifold their energies equal $-(3\Delta/8)\pm\epsilon_0''$, where

$$\epsilon_0''=\tfrac{1}{2}(3\epsilon_0'^2+\epsilon_0^2)^{1/2} \quad \text{(B20)}$$

is the strain-dependent part of the hole energy.